Environmental Science
Water Research & Technology

Capacitive Deionization Using Symmetric Carbon Electrode Pairs

Journal:	*Environmental Science: Water Research & Technology*
Manuscript ID	EW-ART-12-2018-000957.R1
Article Type:	Paper
Date Submitted by the Author:	12-Feb-2019
Complete List of Authors:	gao, xin; University of Kentucky , Center for Applied Energy Research Omosebi, Ayokunle; University of Kentucky, Center for Applied Energy Research Ma, Zilong; University of Kentucky , Center for Applied Energy Research; China University of Mining and Technology Zhu, Feng; University of Kentucky , Center for Applied Energy Research Landon, James; University of Kentucky, Center for Applied Energy Research Ghorbanian, Mahyar; LG&E and KU Energy LLC Kern, Neil; Duke Energy Corp Liu, Kunlei; University of Kentucky, Center for Applied Energy Research

Capacitive Deionization Using Symmetric Carbon Electrode Pairs

X. Gao,[a,*] A. Omosebi,[a] Z. Ma,[a,b] F. Zhu,[a] J. Landon,[a,*] M. Ghorbanian,[c] N. Kern,[d] and K. Liu [a,e,*]

[a]: University of Kentucky Center for Applied Energy Research, Lexington, KY 40511, USA

[b]: National Center for Coal Preparation and Purification Engineering Research, China Mining University of Technology, Jiangsu 221116, China

[c]: Technology Research & Analysis, LG&E and KU Energy LLC, Louisville, KY 40202, USA

[d]: Emerging Technology Office, Duke Energy, Charlotte, NC 28202, USA

[e]: Department of Mechanical Engineering, University of Kentucky, Lexington, KY 40506, USA

*: Xin.Gao1@uky.edu, James.Landon@uky.edu, and Kunlei.Liu@uky.edu

Abstract

A commercially available carbon cloth electrode is repetitively oxidized using a wetting-drying procedure in order to enhance its negative chemical surface charge, consequently creating scenarios of symmetric electrode pairs with different potentials of zero charge (E_{PZC}) versus potential at short circuit for ion desorption (E_o) in a potential distribution. In literature, this study of capacitive deionization (CDI) for the first time provides a new analytical approach that is capable of estimating the E_{PZC} and potential distribution diagram. The approach leverages the modified Donnan model with chemical surface charge, in which values of chemical surface charge are quantified by investigating the effluent pH at steady state with and without carbon electrode pairs in a flow cell. Results from constant-voltage CDI tests show that, for a symmetric pair of carbon electrodes, ion adsorption-desorption performance becomes efficient when a carbon electrode possesses equal positive and negative chemical surface charges or its net chemical

surface charge is zero. By mapping E_{PZC} and E_o in a potential distribution diagram, ineffective ion adsorption-desorption results from electronic charge consumed to repel co-ions at the intermediate charge storage stage. Additionally, Faradaic reactions at the electrodes are discussed based upon pH responses during CDI charging and discharging.

Water Impact Statement

Combined with the modified Donnan model with chemical surface charge, knowledge of potential distribution provides a new insight that is capable of interpreting performance of a capacitive deionization (CDI) cell. Such knowledge can aid in selecting, developing, modifying, and evaluating capacitive carbon electrodes for the emerging CDI technology.

1. Introduction

Even though the earth is largely covered by water, inadequate access to clean water is becoming one of the most pervasive challenges afflicting people globally.[1] While effective, current desalination technologies such as distillation and membrane-based filtration can be costly to implement and operate. As a consequence, alternatives cost-effective and robust desalination solutions should be encouraged. Capacitive deionization (CDI) is an emerging approach using common carbon materials to electrostatically remove ions from a solution.[2] Previous works have improved CDI via physical-chemical modification of carbon electrodes,[3-9] variation in CDI cell architectures,[2, 10-14] mitigation of Faradaic reactions and performance degradation,[15-21] optimization of charging-discharging methods,[22-25] and development of CDI theories.[26-30] Such efforts have made CDI attractive over current desalination technologies, *e.g.*, substantial

minimization of heat treatment, high-pressure pumps, and chemical additives, leading to a significant reduction in capital and operating costs for desalination.[2]

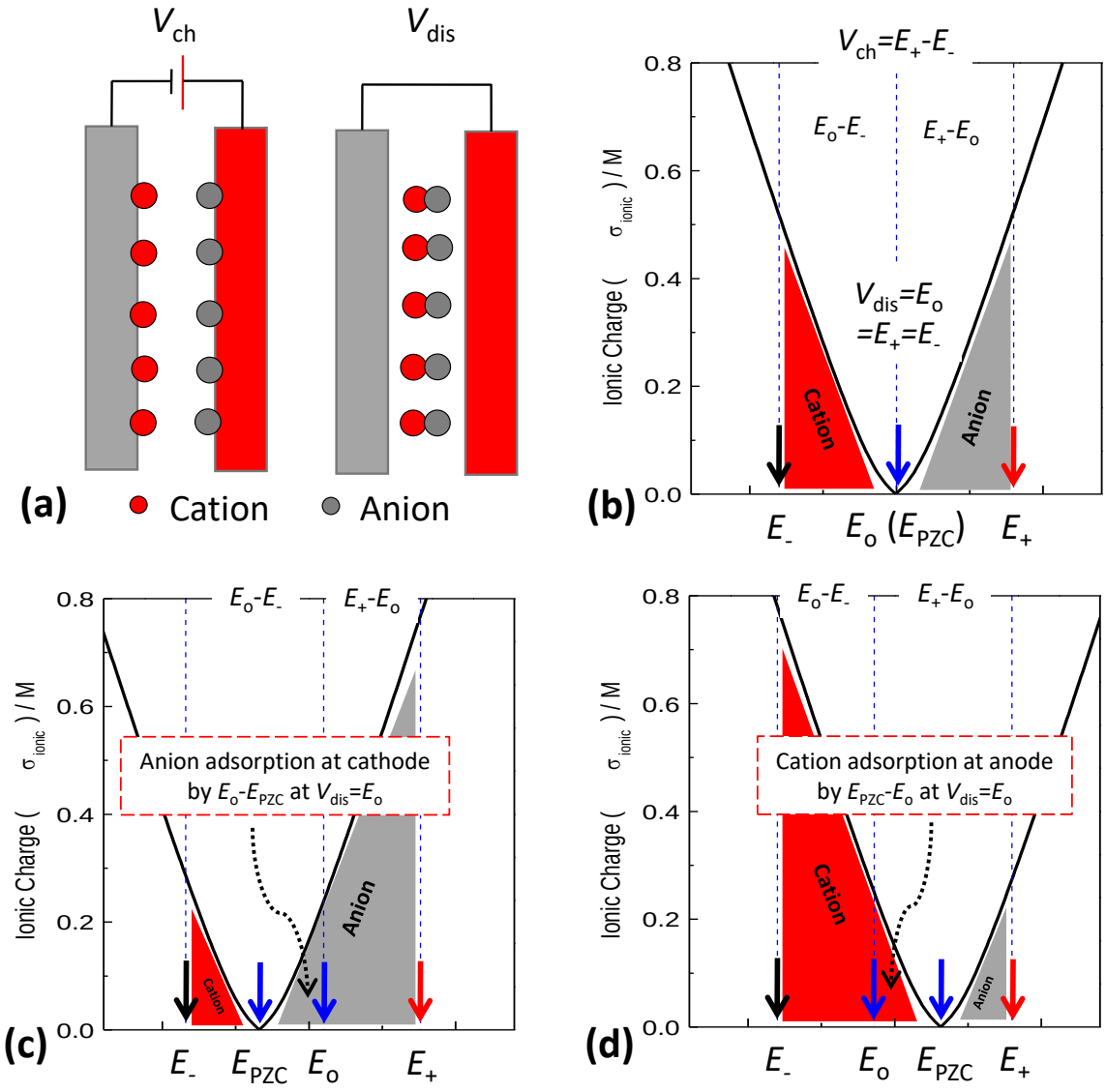

Figure 1. (a) Constant-voltage operation of a CDI cell including a charging voltage (V_{ch}) for ion adsorption and a discharge voltage (V_{dis}) for ion desorption, and its operational mechanism is presented in a potential distribution diagram in (b). (b)-(d) For a symmetric electrode pair, *i.e.*, both the anode and cathode possess the same physical-chemical properties, modifying the chemical

surface charge of the carbon electrode changes the location of potential of zero charge (E_{PZC}) with respect to the potential at short circuit (E_o), thereby impacting the salt removal effectiveness of a CDI cell. In these plots, ionic charge curves are generated using the modified Donnan model with the parameters shown in the caption of Fig. 7, and E_+ and E_- denote the potentials at the anode and cathode, respectively.

Desalination with CDI is achieved in a flow cell with a pair of carbon electrodes separated by a water channel as sketched in Fig. 1(a). Often, constant-voltage operation is adopted to investigate the performance of a CDI cell with a charging voltage (V_{ch}) for ion adsorption and a discharge voltage (V_{dis}) for ion desorption. Details are illustrated by using an ionic charge curve plotted in a potential distribution diagram, where the ionic charge curve is defined by the modified Donnan (mD) model with chemical surface charge for a single carbon electrode according to reference ([26]). It can be seen in Fig. 1(b) that V_{ch} is distributed to the potentials at the anode (E_+) and cathode (E_-), creating two driving/electrostatic forces with respect to the potential at the short circuit (E_o), $E_+ - E_o$ and $E_o - E_-$, to store respective ionic charge into the carbon micropores. To release ions at discharging, the anode and cathode are shorted resulting in $E_+ = E_- = E_o = V_{dis}$ (or $E_+ - E_- = V_{dis} = 0$).

Ion adsorption-desorption by electrodes in a CDI cell depends on the potential of zero charge (E_{PZC}) with reference to E_o within a potential distribution diagram,[31-33] where E_{PZC} typically defines a potential when an electrode has the least ion adsorption.[34, 35] The E_{PZC} is highlighted at the lowest point on the ionic charge curves in Fig. 1(b)-(d) for common CDI cell configurations with symmetric electrode pairs, *i.e.*, both the anode and cathode have the same E_{PZC} and porosity, and where such cells utilize constant-voltage operation discussed above. As shown in Fig. 1(b),

when $E_+ = E_- = E_o = E_{PZC}$ for ion desorption at V_{dis}, no ionic charge will be retained at each electrode. In contrast, cases in Fig. 1(c) and (d) suggest that the electrode can store ionic charge at V_{dis} since E_{PZC} and E_o are found in different locations, *e.g.,* the cathode adsorbs anions in Fig. 1(c) by the driving force of E_o - E_{PZC} at $V_{dis} = E_o$. Furthermore, these cases result in unequal driving forces at the anode and cathode by counting the ionic charge, which will be detailed in section 3.5.

In this work, scenarios for different E_{PZC} locations versus E_o in a potential distribution diagram for symmetric electrode pairs is created via oxidizing a commercially available carbon cloth electrode. Importantly, for the first time in the literature of CDI, a new insight is provided to estimate the E_{PZC} and predict the potential distribution using the mD model with chemical surface charge, in which values of chemical surface charge are quantified by investigating the effluent pH at steady state with and without carbon electrode pairs in a flow cell. Finally, through these efforts, it is considered that knowledge of the potential distribution combined with charge balances is capable of interpreting and predicting the performance for CDI cells.

2. Material and Methods

2.1. Electrode Preparation

To facilitate our discussion, carbon electrodes used in the present work are denoted electrodes A, B, and C with different chemical surface charges. Electrode A, a microporous carbon cloth electrode that was purchased from Engineered Fibers Technology, Connecticut, USA, was directly used in the experiments without treatment. Previous results depict that this electrode possessed positive chemical surface charge in NaCl solution.[21] Therefore, to enhance its negative chemical surface charge but without bringing additional chemical species such as nitrate, NO_3^-, carbon

oxidation was carried out using deionized water to wet electrode A followed by air-drying at 280°C for 24 hours, as similarly performed in reference ([36]). Electrodes B and C were the resulting electrodes from 3 and 7 times repetitive oxidation, respectively, via the wetting-drying procedure introduced above.

2.2. Pore Volume and Surface Functional Groups

Surface functional groups were studied using a Nicolet 6700 Fourier-transform infrared (FTIR) spectrometer. The mixing ratio of electrode to KBr was 0.3 wt%, of which 70 mg of the mixture was milled and pressed to form a pellet. FTIR spectra including KBr background were recorded by co-adding 256 scans at 4 cm^{-1} resolution under N_2 environment. Pore volume was quantified using a Micromeritics ASAP2020 surface area and porosity analyzer. Approximately 100 mg of electrode was degassed at 120°C under vacuum for 12 hours, and N_2 adsorption-desorption isotherms were recorded at 77 K. The non-localized density functional theory was used to calculate the cumulative pore volume as a function of pore size, as it generally accommodates various pore geometries.[37]

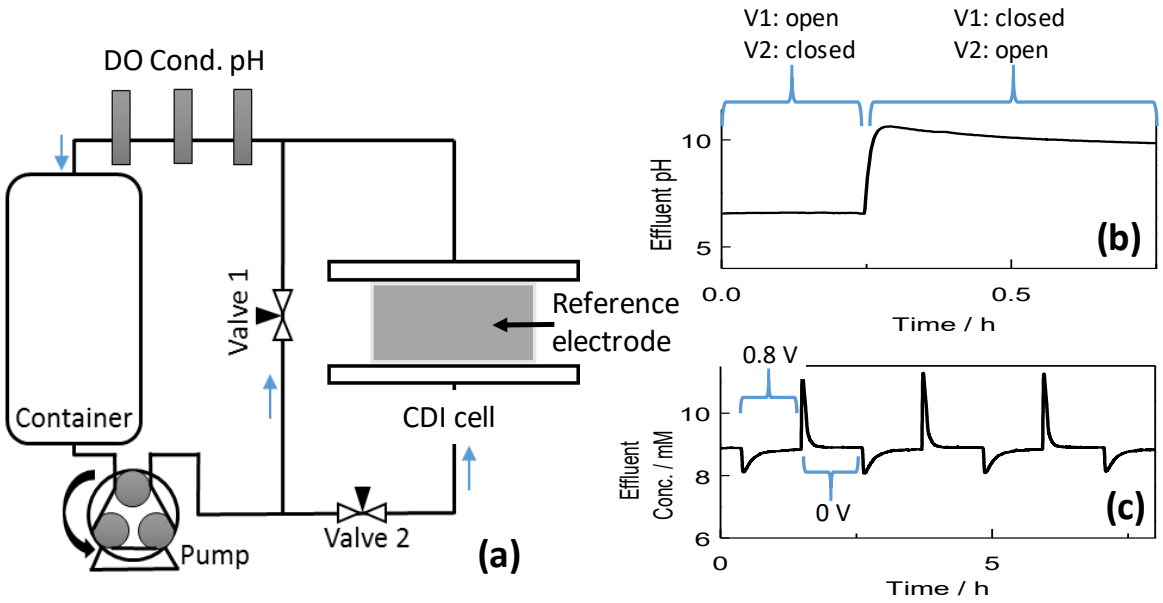

Figure 2. (a) Monitoring effluent pH, conductivity, dissolved oxygen (DO), and potentials at electrodes of a CDI cell. During the tests, (b) without applying voltage, electrode surface charge was first identified by monitoring changes in the effluent pH when NaCl solution passes through or bypasses the CDI cell via opening or closing valves 1 and 2, (c) followed by CDI charging and discharging when closing valve 1 and opening valve 2. Unless stated otherwise, surface charge testing was performed in 31 L of 9 mM deaerated NaCl solution at 90 mL min^{-1} followed by CDI testing at 0.8 V charging and 0 V discharging in the same NaCl solution at 25 mL min^{-1}.

2.3. Chemical Surface Charge and CDI Testing

Fig. 2(a) shows the setup used for both the chemical surface charge and CDI tests. This setup included a homemade flow-through CDI cell with carbon electrodes adjacent to titanium current collectors, two polyethylene needle valves, Thermo Scientific pH, conductivity, and dissolved oxygen probes, a homemade polyethylene tank, and a Cole-Parmer Masterflex L/S peristaltic pump. As similarly performed in reference ([11, 18]), a saturated calomel electrode (SCE) was used to measure potentials across the electrodes during testing, where the SCE was parallel to the electrodes. Mass of the dry electrode pairs A-C in both the surface charge and CDI tests were about 2.9, 2.4, and 2.2 g, respectively. Each test used freshly prepared 31 L of 9 mM NaCl solution that was circulated at 90 mL min^{-1} for surface charge tests and 25 mL min^{-1} for CDI tests while flushing with gaseous N_2.

The procedure for surface charge testing is demonstrated in Fig. 2(b). By opening valve 1 and closing valve 2, pH of the bulk solution at steady state was first measured without the CDI cell. Subsequently, by closing valve 1 and opening valve 2, the dry electrode pairs in the CDI cell were wetted. Due to different surface interactions with water at the carbon electrodes (see reactions

(10) and (11)), the effluent pH after the CDI cell was modified toward a new steady-state value. Under such a condition, along with references ([38-40]), the net positive and negative chemical surface charges, $\sigma_{chem,+}$ and $\sigma_{chem,-}$, are estimated using the effluent pH of the CDI cell at steady state via

$$\sigma_{\mathrm{chem},+} = (10^{(\mathrm{pH}-14)}V_{\mathrm{sol}})/(v_{\mathrm{mic}}m) \quad (1)$$

$$\sigma_{\mathrm{chem},-} = (10^{(-\mathrm{pH})}V_{\mathrm{sol}})/(v_{\mathrm{mic}}m) \quad (2)$$

where V_{sol} is the volume of solution, v_{mic} is the micropore volume of electrode, and m is the weight of electrode. It is noted that equations (1) and (2) are valid when solution is alkaline and acidic, respectively, suggesting that net chemical surface charge of a carbon electrode will be 0 if the effluent pH value is 7.

Following the surface charge test, without dissembling the CDI cell and changing solution, CDI testing was performed at 0.8 V charging and 0 V discharging (0.8/0 V) to study CDI performance, as illustrated in Fig. 2(c). Time taken for each charging and discharging step was 2,000 s. Due to using a large volume of solution, effluent concentration at equilibrium after the salt adsorption and desorption is approximately equivalent to the concentration of the bulk solution (c_{salt}). Therefore, salt adsorption capacity at equilibrium (SAC) is calculated by multiplying the volumetric flow rate (Φ) by integration of the effluent concentration (c(t)) with time (t) via

$$\mathrm{SAC} = (M_{\mathrm{w}}\Phi/m)\int\big(c_{\mathrm{salt}} - c(\mathrm{t})\big)\mathrm{dt} \quad (3)$$

where M_w is the molar mass of NaCl. The corresponding electronic charge pass (Q) is calculated by integrating the specific current curve resulting from the measured current divided by m, in

which *m* is 2.9, 2.4, and 2.2 g for electrode pairs A, B, and C, respectively. Finally, the charge efficiency (Λ) is

$$\Lambda = (\Gamma F)/(MQ) \quad (4)$$

where *F* is Faraday's constant.

2.4. Modified Donnan Model with Chemical Surface Charge

The mD model for 1:1 salt solution was used to estimate E_{PZC}, aiding greatly in discussing the potential distribution in section 3.5. As learned from references ([3, 26]), it is assumed that, for a porous carbon electrode, σ_{chem} is balanced by both electronic charge (σ_{elec}) and ionic charge (σ_{ionic}), *i.e.*,

$$\sigma_{ionic} + \sigma_{elec} + \sigma_{chem} = 0 \quad (5)$$

σ_{ionic} and σ_{elec} relate to the Donnan potential ($\Delta\Phi_D$) and the Stern potential ($\Delta\Phi_S$) via

$$\Delta\Phi_D = -\text{arcsinh}(\sigma_{ionic}/2c_{salt}) \quad (6)$$

$$\Delta\Phi_S = (\sigma_{elec}F)/(C_S V_T) \quad (7)$$

where V_T is the thermal voltage and C_S is the Stern capacitance. Consequently, potential at an electrode (*E*) is expressed as

$$E = (\Delta\Phi_D + \Delta\Phi_S)V_T \quad (8)$$

In the mD model, total ion concentration in the micropores ($c_{T,ions}$) is given by

$$c_{T,ions}^2 = \sigma_{ionic}^2 + 4c_{salt}^2 \quad (9)$$

Equations (5)-(9) suffice to estimate E_{PZC} in a plot of σ_{ionic} as a function of E for an electrode when σ_{chem}, c_{salt}, C_S, and V_T are fixed in the mD model.

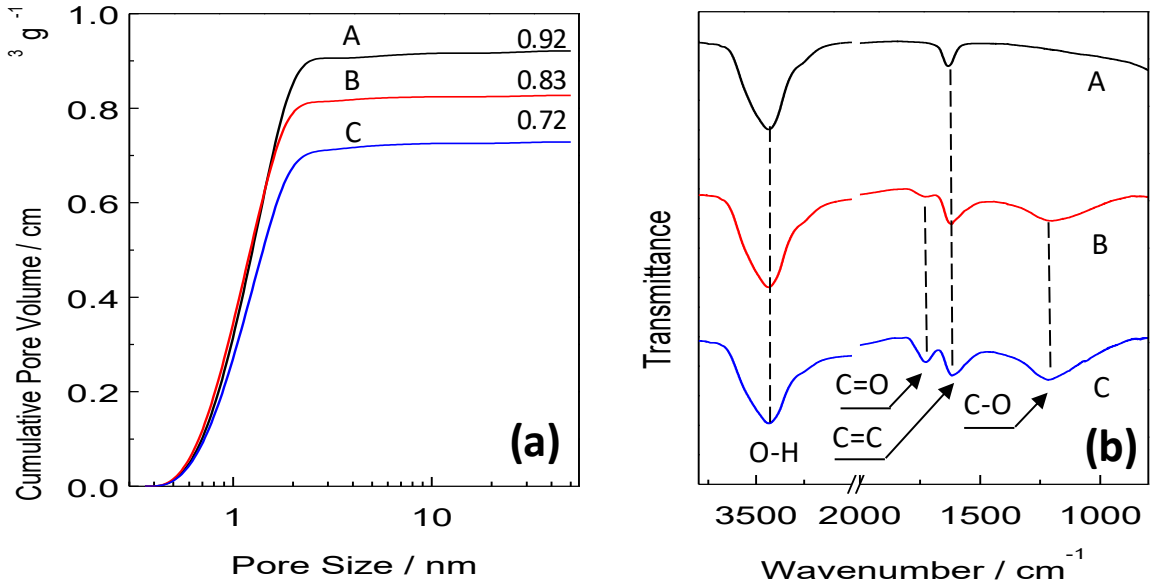

Figure 3. Characterizations of electrodes A-C. (a) Cumulative pore volumes. (b) FTIR spectra.

3. Results and Discussion

3.1. Porosity and Surface Functional Groups

Cumulative pore volumes versus pore size for electrodes A-C are plotted in Fig. 3(a). Overall, each plot possesses a sharp increase in the cumulative pore volume below 2 nm and a flat region above 2 nm, indicating the retained microporous structures of electrodes B and C resulting from repetitive oxidations in comparison of electrode A. However, the total pore volume evaluated at pore sizes up to 50 nm decreases, *i.e.*, electrodes A, B, and C have the total pore volume of 0.92, 0.83, and 0.72 mL g^{-1}, respectively. Fig. 3(b) shows the FTIR spectra of electrodes A-C as expressed in terms of transmittance. Without treatment, electrode A has bands for O-H stretching at 3430 cm^{-1}

and C=C stretching at 1600 cm^{-1}.[41, 42] After treatment, newly formed bands depict modifications in the surface functional groups of electrodes B and C, *i.e.*, bands formed at 1730 and 1200 cm^{-1} denote C=O and C-O stretching, respectively,[41, 42] suggesting the presence of carboxylic groups, -COOH, due to carbon oxidation. Additionally, compared to electrode B, carbon-oxygen related bands associated with electrode C become more significant due to the increased repetition of carbon oxidation.

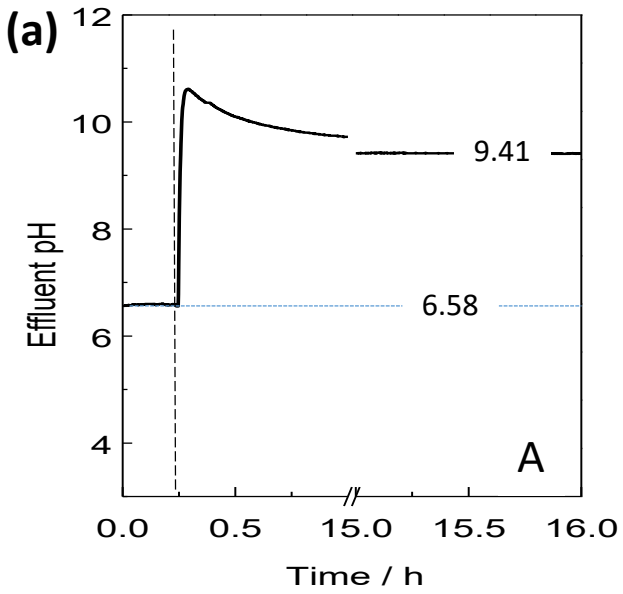
(a)
Effluent pH
12
10
8
6
4
9.41
6.58
A
0.0
0.5
15.0
15.5
16.0
Time / h

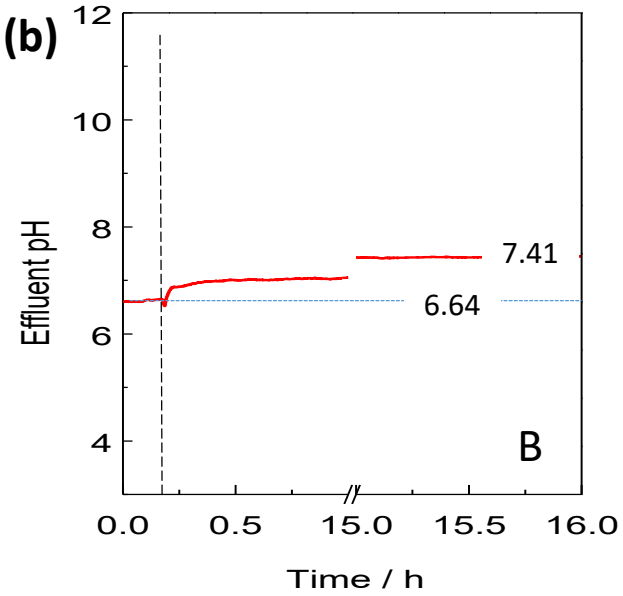
(b)
Effluent pH
12
10
8
6
4
7.41
6.64
B
0.0
0.5
15.0
15.5
16.0
Time / h

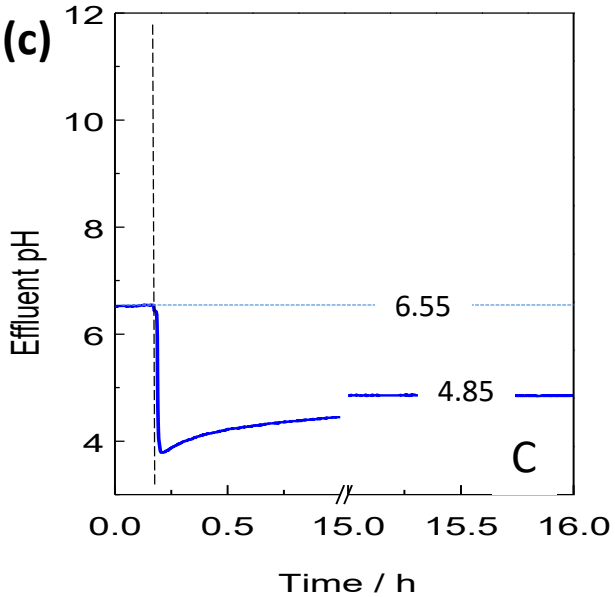
(c)
Effluent pH
12
10
8
6
4
6.55
4.85
C
0.0
0.5
15.0
15.5
16.0
Time / h

Figure 4. (a)-(c) Changes in the effluent pH via opening or closing valves 1 and 2 (see Fig. 2) to identify surface charge conditions of electrodes A-C, respectively. In plots (a)-(c), the effluent pH at the left (right) side of the dashed line was measured when opening (closing) valve 1 and closing (opening) valve 2. Therefore, changes in the effluent pH reflect the charged surface conditions at the electrodes.

3.2. Identification of Surface Charged Sites by Effluent pH

Surface charged sites of electrodes A-C were identified by monitoring changes in the effluent pH using the setup in Fig. 2 without applying any voltage to the CDI cell. As shown in Fig. 4, when solution bypasses the CDI cell via opening valve 1 and closing valve 2, pH of the solution at the left side of the dashed lines is 6.60. Due to different interactions at the surface of the electrodes, effluent pH of the CDI cell configured with electrodes A-C respond differently when closing valve 1 and opening valve 2. For example, at the right side of the dashed line in Fig. 4(a), electrode A displays an increase in the effluent pH with a near steady-state value of 9.41. According to reference ([36, 39]), such an increase is because the basal planes of carbon (C_π) behave as a Lewis base with its acid-base reaction of

$$-C_{\pi(\text{surface})} + 2H_2O \rightarrow -C_\pi H_3O^+_{(\text{surf})} + OH^- \qquad (10)$$

thereby resulting in not only an increased pH but also positively charged sites at electrode A. Under this circumstance, negatively charged species such as Cl^- can be adsorbed at the electrode surface.[38]

In contrast to electrode A, electrode B depicts a decreased effluent pH with a steady-state value of 7.41 in Fig. 4(b). Under such a condition, according to reference ([39]), -COOH formed by carbon oxidation acts as Brönsted acid with the reaction of

$$-\mathrm{COOH}_{(\mathrm{surface})} + \mathrm{H_2O} \rightarrow -\mathrm{COO}^-_{(\mathrm{surf})} + \mathrm{H_3O}^+ \quad (11)$$

thus contending with reaction (10) to neutralize the effluent pH while compromising the positive surface charged sites at electrode B. As the repetition of carbon oxidation increases, in Fig. 4(c), effluent pH of electrode C further drops to a steady-state value of 4.85, which suggests that reaction (11) becomes dominant. Consequently, more negatively charged sites are produced at the surface of electrode C.

According to both the total pore volume and pH values in Fig. 3 and 4, $\sigma_{chem,+/-}$ are estimated via equations (1) and (2) with respect to the neutral condition at pH of 7, yielding net chemical surface charges of ~0.30 M for electrode A, ~0 M for electrode B, and ~-0.28 M for electrode C, of which electrode B displays quite balanced positive and negative chemical surface charges. Additionally, these values will be used in the mD model to locate the E_{PZC} in a plot of σ_{ionic} as a function of E, aiding in discussion regarding the potential distributions measured during charging and discharging when symmetric electrode pairs A-C are configured in a CDI cell.

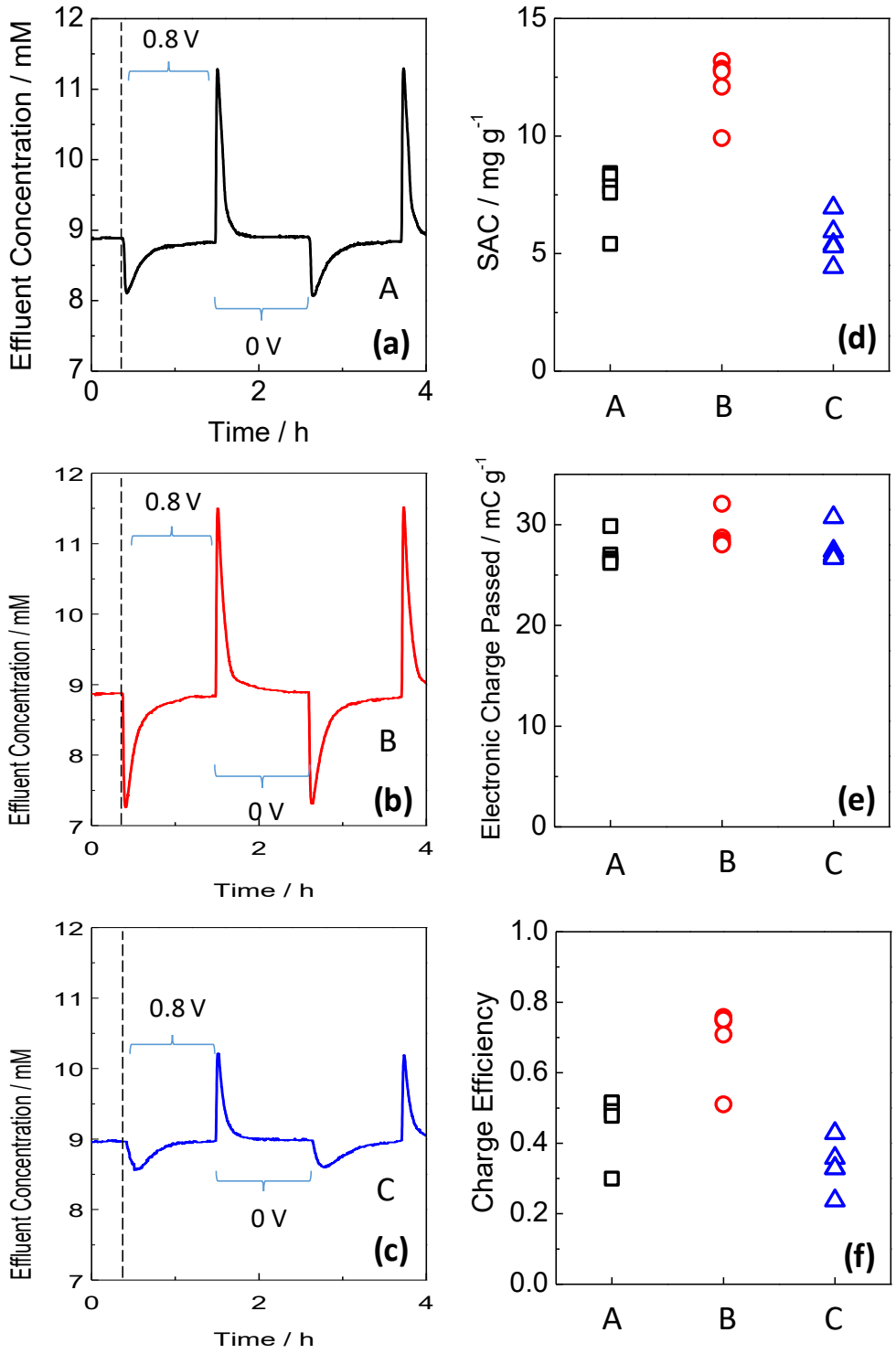

Figure 5. (a)-(c) Effluent concentration of the 1st and 2nd cycles at 0.8/0 V when a CDI cell was configured with electrode pairs A-C. The effluent concentration at the left side of the dashed line

was measured before charging the CDI cell. (d)-(f) Performance evaluations using equations (3) and (4) based upon the plots of (a)-(c). The corresponding current profiles are depicted in Fig. S1(d)-(f). It is noted that, in Fig. 5(d)-(f), the first cycles for all of the electrode pairs possess the lowest SAC and charge efficiency values but highest electronic charge passed values compared to those associated with the remaining cycles.

3.3. CDI Testing and Performance Evaluation

After identifying surface charged sites in section 3.2, CDI testing was subsequently performed at 0.8/0 V to study salt removal without disassembling the CDI cell and changing the NaCl solution. Typical effluent concentration profiles are observed in Fig. 5(a)-(c), in which salt adsorption at 0.8 V is reflected by a temporal decrease in effluent concentration, and vice versa for desorption at 0 V. According to both the effluent concentration and current profiles in Fig. S1(d)-(f), SAC, electronic charge passed, and charge efficiency are calculated for each electrode pair using equations (3) and (4). As shown in Fig. 5(d), a higher SAC of 12.5 mg g^{-1} is obtained from electrode B in comparison to 7.5 mg g^{-1} for electrode A and 5.6 mg g^{-1} for electrode C. Similarly, in Fig. 5(f), electrode B offers a higher charge efficiency of ~75%, as no significant difference in the electronic charged pass is observed in Fig. 5(e). Moreover, Fig. S3 presents a CDI Ragone plot based upon the first adsorption half cycles in Fig. 5(a)-(c), suggesting a higher SAC and rate associated with electrode pair B in comparison to that for electrode pairs A and C.[43]

Surface charged sites, Faradaic reactions, and conductivity of flow cells assembled with carbon electrodes generally affect salt removal of a CDI cell.[3, 19, 44] In the present study, the latter two effects are considered to be substantially reduced, *i.e.*, solution was continuously purged with N_2 gas to deplete most of the dissolved oxygen (see Fig. S2(a)-(c)), a relatively small charging

voltage, 0.8 V, was also selected to substantially minimize Faradaic reactions, *e.g.*, dissolved oxygen reduction at the cathode and carbon oxidation at the anode, and the conductivity of the CDI cell configured with electrode pairs A-C was very similar (see similar peak currents at the onset of charging in Fig. S1(d)-(f)). As a consequence, the superior CDI performance associated with electrode pair B should be attributed to the nearly balanced positive and negative surface charges, σ_{chem} = ~0 M, as characterized in section 3.2.

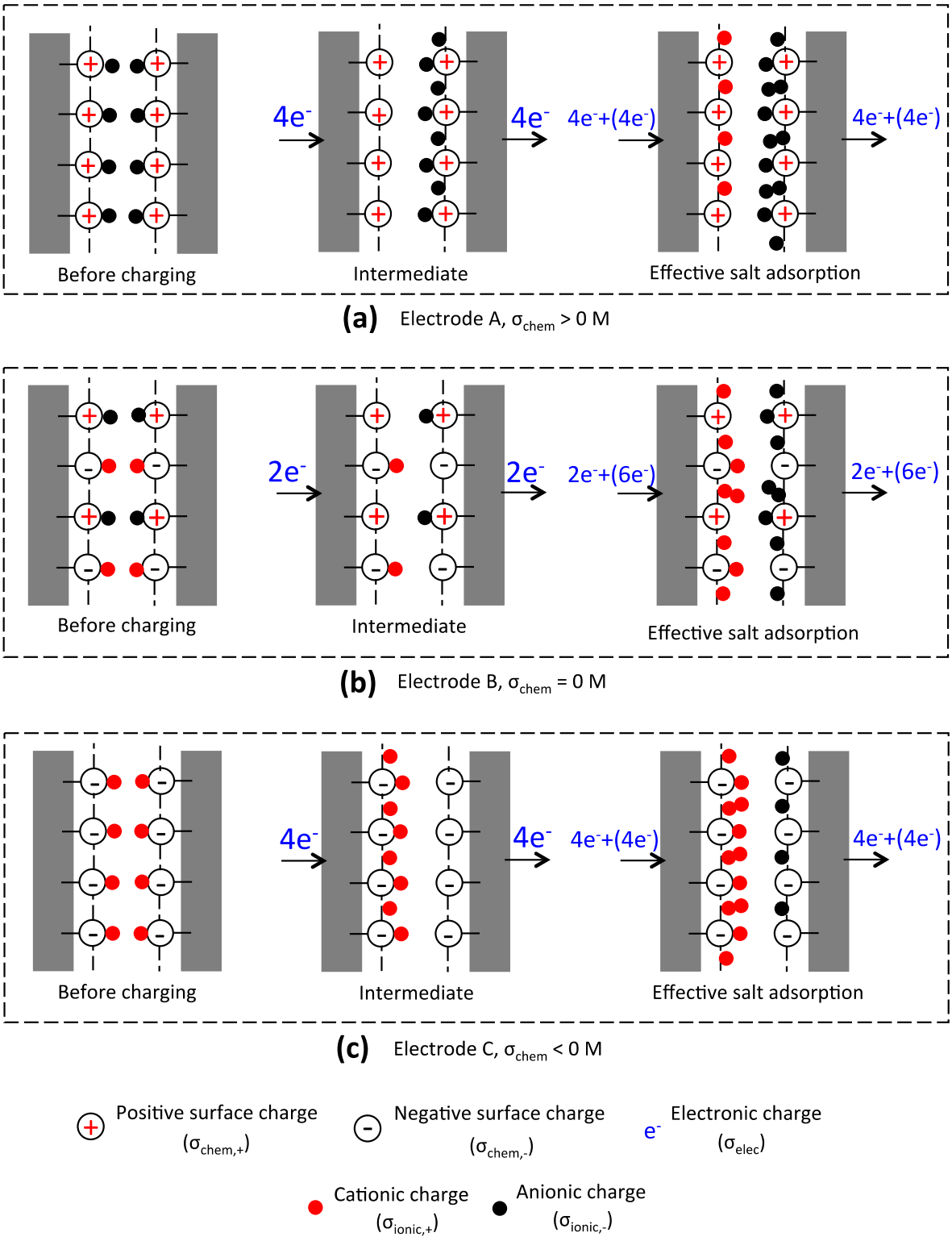

Figure 6. Salt adsorption affected by surface charged sites for symmetric electrode pairs, including (a) electrode A with $\sigma_{chem} > 0$ M, (b) electrode B with $\sigma_{chem} = 0$ M, and (c) electrode C with σ_{chem}

< 0 M. In each scenario, it is assumed that (1) only 8 σ_{elec} are used to balance ionic and chemical surface charges without considering Faradaic reactions, and (2) surface charged sites are the same for all of the electrodes. It is noted that, at the stage of effective salt adsorption, electronic charge in the parentheses is used for net salt adsorption.

3.4. Net Charge Adsorption Affected by Chemical Surface Charge

To support the conclusion mentioned above, Fig. 6 provides three scenarios concerning the balance of chemical surface, ionic, and electronic charges, pertaining to (a) $\sigma_{chem} > 0$ M for electrode A, (b) $\sigma_{chem} = 0$ M for electrode B, and (c) $\sigma_{chem} < 0$ M for electrode C. It is generally assumed that (1) each scenario is composed of three stages of ion adsorption including before charging, intermediate, and effective salt adsorption; (2) total number of σ_{elec} used to balance cationic/anionic charges ($\sigma_{ionic,+/-}$) and positive/negative surface charge ($\sigma_{chem,+/-}$) is 8, the same for each scenario, as the electronic charge passed in Fig. 5(e) is relatively equal; and (3) there is minimal interruption of charge transfer owing to Faradaic reactions, as the solution was deaerated to mitigate dissolved oxygen reduction and corresponding carbon oxidation at the anode.[17, 45]

Fig. 6(a) depicts a scenario representing the surface charge sites of electrode A, *i.e.*, $\sigma_{chem} > 0$ M, in which 4 $\sigma_{chem,+}$ are set at each electrode, therefore requiring 4 $\sigma_{ionic,-}$ to retain electroneutrality before charging. At the onset of charging, an intermediate stage occurs in which 4 σ_{elec} are injected into the cathode to repulse 4 $\sigma_{ionic,-}$ into solution, thus balancing 4 $\sigma_{chem,+}$ at the cathode. Under such an intermediate stage, there is no ionic charge stored at the carbon surface, and the relevant potential at the carbon electrode defines the potential of zero (ionic) charge, E_{PZC}. Meanwhile, 4 $\sigma_{ionic,-}$ from solution are stored at the anode. Subsequently, effective salt adsorption occurs as additional 4 σ_{elec} is used to adsorb 4 $\sigma_{ionic,+}$ at the cathode, paired with attraction of 4

$\sigma_{ionic,-}$ at the anode. Overall, this scenario gives a loss of 50% σ_{elec} during the intermediate stage, and the remaining 50% contributes to net salt adsorption.

Fig. 6(b) presents a scenario corresponding to the surface charged sites of electrode B, *i.e.*, $\sigma_{chem} = 0$ M. Before charging, each electrode possesses 2 $\sigma_{chem,+}$ and 2 $\sigma_{chem,-}$, thus attracting 2 $\sigma_{ionic,-}$ and 2 $\sigma_{ionic,+}$ to retain electroneutrality. In contrast to solely $\sigma_{ionic,-}$ transfer in Fig. 6(a) during the intermediate stage, 2 $\sigma_{ionic,-}$ at the cathode are repulsed by 2 σ_{elec}, coupled with 2 $\sigma_{ionic,+}$ being released at the anode, leading to net salt desorption, a similar mechanism to inverted CDI. However, this inverted behavior is not shown by the conductivity probe in the present experiment due to the use of larger constant-voltage for charging. As an additional 6 σ_{elec} are injected, 6 $\sigma_{ionic,+}$ paired with 6 $\sigma_{ionic,-}$ contribute to net salt adsorption, thus 2 more ionic pairs are removed when compared to that in Fig. 6(a). As a result, the scenario demonstrates that 25% σ_{elec} is consumed during the intermediate stage, and 75% σ_{elec} is utilized for net/effective salt adsorption. Fig. 6(c) depicts a scenario associated with the surface charge sites of electrode C, *i.e.*, $\sigma_{chem} < 0$ M, as completely opposed to the charged configuration in Fig. 6(a). However, by balancing all of the charges, this scenario also expends 50% σ_{elec} on solely $\sigma_{ionic,+}$ transfer at the intermediate stage, the same value as presented in Fig. 6(a).

In summary, by counting the number of charges, Fig. 6 pictorially demonstrates that, when an electrode has balanced positive and negative charged sites, losses in σ_{elec} at the intermediate stage is minimized toward more effective salt adsorption.

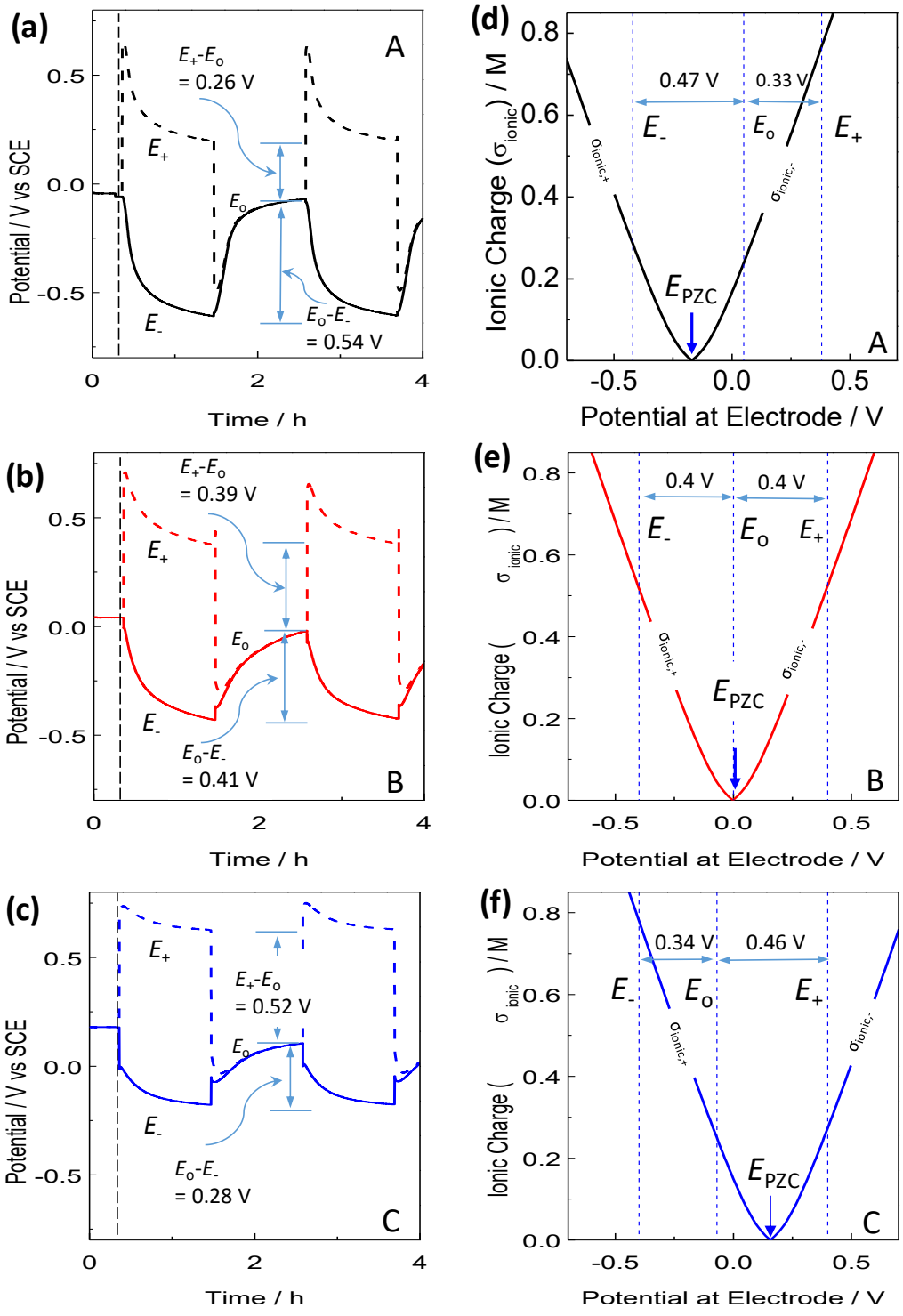

Figure 7. (a)-(c) Potential distributions that were simultaneously measured during the CDI tests in Fig. 5(a)-(c). (d)-(f) Using the mD model to demonstrate changes in the potential distributions

in the plots of (a)-(c). Parameters used in the model are C_s = 170 F mL^{-1}, c_{salt} = 9 mM, V_T = 0.0256 V, σ_{chem} = 0.30, 0, and -0.28 M for electrode pairs A-C, respectively, and v_{tot} = 0.92, 0.83, and 0.72 cm^3 g^{-1} for electrode pairs A-C, respectively. In these plots, E_+, E_-, E_o, and E_{PZC} denote the potentials at the anode, cathode, short circuit, and zero ionic charge, respectively.

3.5. Potential Distribution Affected by Chemical Surface Charge

Ion adsorption-desorption requires driving forces at the electrodes in a CDI cell. In this section, discussion is focused on the effect of chemical surface charge on the potential distribution. Fig. 7(a)-(c) show the potential distributions that were simultaneously measured during the CDI tests in Fig. 5(a)-(c), where E_+, E_-, and E_o denote the potentials at the anode, cathode, and short circuit, respectively. Overall, during charging for salt adsorption, the cell voltage of 0.8 V is distributed to E_+ and E_-, while during discharging for salt desorption, E_+ and E_- are merged leading to $E_+ = E_- = E_o$. As highlighted in Fig. 7(a) for electrode pair A, potential across the anode, $E_+ - E_o$ (= 0.26 V), for anion adsorption is much smaller than potential across the cathode, $E_o - E_-$ (= 0.54 V), for cation adsorption. With enhancing $\sigma_{chem,-}$, electrode pair B in Fig. 7(b) displays that $E_+ - E_o$ (= 0.39 V) nearly equals $E_o - E_-$ (= 0.41 V). However, in Fig. 7(c) for electrode pair C, $E_+ - E_o$ (= 0.52 V) is greater than $E_o - E_-$ (= 0.28 V), an opposite case to Fig. 7(a), owing to completely different σ_{chem} between electrodes C and A. As expected in a two-electrode system such as a CDI cell, the more sluggish electrode demands a higher driving force to counter its ineffective charge transfer,[34] pertaining to the balance of ionic charge at the intermediate stage in Fig. 6. To connect the knowledge of driving force and charge transfer, the mD model is used to construct ionic charge curves in a potential distribution using the parameters depicted in the caption of Fig. 7, in which the ionic charge is defined as moles of charge per micropore volume.

Fig. 7(d)-(f) illustrate the use of the mD model to set the E_{PZC} for electrodes A-C on the E axis, in which σ_{ionic} at E_{PZC} is 0. With respect to E_{PZC}, E_o, E_+, and E_- are assigned in the plots, in agreement with the surface charge scenarios that have been presented in Fig. 6. For instance, as noted in Fig. 6(a), due to electrode A that possesses $\sigma_{chem,+}$ balanced or covered with $\sigma_{ionic,-}$ before charging, its E_o should be greater than E_{PZC} in Fig. 7(d). As charging begins, E_- moves across E_{PZC} from E_o, thus creating two potential differences, $E_o - E_{PZC}$ and $E_{PZC} - E_-$ at the cathode. Under such a condition, coupled with $E_+ - E_o$ at the anode for $\sigma_{ionic,-}$ adsorption, σ_{elec} generated by $E_o - E_{PZC}$ repels $\sigma_{ionic,-}$ to balance $\sigma_{chem,+}$ at the intermediate stage, while another σ_{elec} by $E_{PZC} - E_-$ contributes to $\sigma_{ionic,+}$ adsorption towards net salt adsorption. This potential-charge reconciliation is also valid for the placement of potentials for electrodes B and C in Fig. 7(e) and (f), respectively. Through this analysis, it is believed that the potential difference between E_o and E_{PZC}, $|E_o - E_{PZC}|$, is detrimental to σ_{elec} utilization for salt adsorption, thereby limiting CDI performance associated with electrode pairs A and C.

$|E_o - E_{PZC}|$ causes the unbalanced potential distributions observed here. To support this conclusion, a procedure to set E_o, E_+, and E_- on the E axis is presented based upon the balance of charges as discussed above. Along with electrode pair A in Fig. 7(d) as an example, this procedure includes: (1) the mD model is first used to plot σ_{ionic} versus E of electrode A in Fig. 7(d) with the parameters as depicted in the caption of Fig. 7; (2) SAC of 7.5 mg g^{-1} for electrode A is converted to σ_{ionic} via $\sigma_{\mathrm{ionic}} = \sqrt{(c_{\mathrm{T,ions}}^2 - 4c_{\mathrm{salt}}^2)}$, where $c_{T,ions}$ = 2SAC/($M_w \nu_{mic}$) and c_{salt} = 9 mM; (3) the σ_{ionic} calculated from step (2) is used to locate potential at the electrode that limits CDI performance in Fig. 7(d), *e.g.*, E_- = –0.42 V at $\sigma_{ionic,-}$ = 0.28 M; (4) subtracting the potential obtained from step (3) from the applied voltage of 0.8 V yields potential at the counter electrode, *e.g.*, E_+ = 0.38 V; (5) the potential calculated from step (4) is used to find the corresponding σ_{ionic}, *e.g.*, $\sigma_{ionic,+}$ = 0.77

M at E_+ = 0.38 V; and finally, (6) difference between the σ_{ionic} resulting from steps (5) and (2) is the $2\sigma_{ionic}$ at E_o, *e.g.*, E_o = 0.05 V at $\sigma_{ionic,+}$ = 0.24 M. Note that the number of 2 in $2\sigma_{ionic}$ stems from σ_{ionic} transfer at the intermediate stage, *e.g.*, one $\sigma_{ionic,-}$ is repulsed from electrode A that serves as the cathode, while another one $\sigma_{ionic,-}$ is adsorbed onto the anode.

By using the procedure above, $E_+ - E_o$ and $E_o - E_-$ are highlighted by the dashed lines in Fig. 7(d)-(f), in which electrodes A and C display unbalanced potential distributions, a similar observation to the measured potential distributions in Fig. 7(a)-(c). Mathematically, an unbalanced potential distribution always occurs unless $E_o = E_{PZC}$, as ΔE versus $\Delta\sigma_{ionic}$ is nonlinear resulting from the hyperbolic function of $\Delta\Phi_D$ in the mD model (See equation (6)). Physically, instead of contributing to ion adsorption, $|E_o - E_{PZC}|$ at the limiting electrode is used to reconcile surface charged sites with σ_{elec}, thereafter causing the potential distribution to be unbalanced.

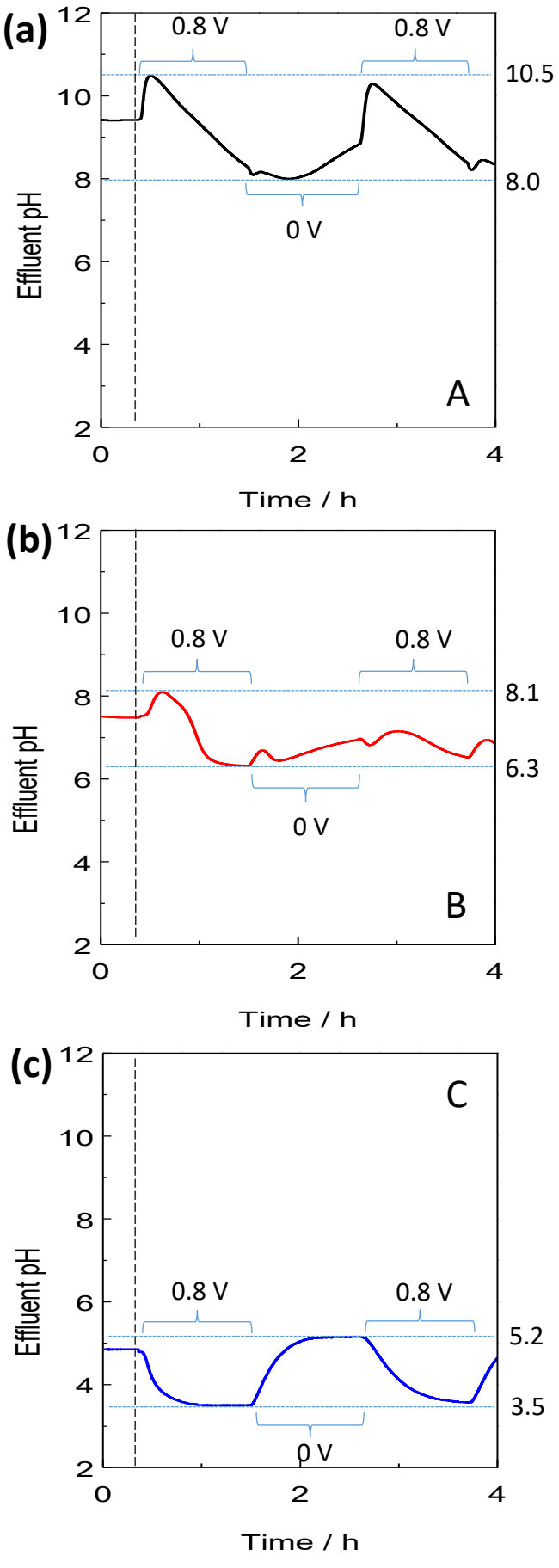
(a)
0.8 V
0.8 V
10.5
8.0
0 V
A
Effluent pH
Time / h
(b)
0.8 V
0.8 V
8.1
6.3
0 V
B
Effluent pH
Time / h
(c)
C
0.8 V
0.8 V
5.2
3.5
0 V
Effluent pH
Time / h

Figure 8. (a)-(c) Effluent pH profiles that were simultaneously measured during salt removal tests in Fig. 5(a)-(c).

3.6. Faradaic Reactions Related to pH Responses

Faradaic reactions in a CDI cell typically include dissolved oxygen reduction at the cathode and carbon oxidation at the anode, which can cause changes in the effluent pH.[17-19, 45] Fig. 8(a)-(c) provide the effluent pH profiles that were simultaneously recorded during the CDI tests in Fig. 5(a)-(c), charging at 0.8 V and discharging at 0 V. Due to very different starting pH values resulting from the surface interactions via equations (10) and (11), effluent pH from electrode pairs A and C are first discussed. As shown in Fig. 8(a), electrode pair A possesses an increased pH segment at the onset of charging followed by a continuously decreasing pH segment until discharging. Because of the alkaline environment, pH > 7, the initial increased pH can be accounted for by $O_{2(dissolved)}$ reduction at the cathode via[17]

$$O_{2(dissolved)} + 2H_2O + 4e^- \rightarrow 4OH^-, E^o = 0.16 \text{ V vs SCE} \quad (12(a))$$

$$O_{2(dissolved)} + H_2O + 2e^- \rightarrow HO_2^- + OH^-, E^o = -0.31 \text{ V vs SCE} \quad (12(b))$$

Even though solution was deaerated during the entirety of the tests, reductions in a small amount of $O_{2(dissolved)}$ were still detectable during charging as depicted in Fig. S2(a)-(c). The latter decreased pH means carbon oxidation at the anode would dominate with the possible reactions of[46]

$$C + H_2O \rightarrow C - O_{ad} + 2H^+ + 2e^- \quad (13(a))$$

$$C - O_{ad} + H_2O \rightarrow COO^-_{(surf)}(H^+) + 2H^+ + 2e^-,\ E^o = -0.03\ V\ vs\ SCE \quad (13(b))$$

By comparing the measured E_o (=-0.07 V vs SCE) in Fig. 8(a) and E^o of reactions (12)-(13), the gradually increased pH during discharging suggests $O_{2(dissolved)}$ can be still reduced at the cathode; on the contrary, carbon oxidation at the anode is minimal.

In contrast to electrode pair A, effluent pH of electrode C in Fig. 8(c) descends initially during charging, meaning that H^+ is produced in the CDI cell. When tested under acidic conditions, pH < 7, reference ([17]) suggests $O_{2(dissolved)}$ reduction at the cathode may follow

$$O_{2(dissolved)} + 4H^+ + 4e^- \rightarrow 4H_2O,\ E^o = 0.99\ V\ vs\ SCE \quad (14(a))$$

$$O_{2(dissolved)} + 2H^+ + 2e^- \rightarrow H_2O_2,\ E^o = 0.43\ V\ vs\ SCE \quad (14(b))$$

accompanied with H^+ consumption. Therefore, it is deduced that the decreased pH is primarily attributed to carbon oxidation at the anode such as reaction (13). As charging progresses, effluent pH is stabilized, possibly due to $O_{2(dissolved)}$ reduction via equation (14) and corresponding carbon oxidation via equation (13). During discharging, effluent pH depicts a mirror image to charging, suggesting that carbon oxidation becomes less active at the anode. Finally, due to the near-neutral feed solution testing condition, effluent pH associated with electrode pair B offers all of the major features in between electrodes A and C, displaying competing reactions between $O_{2(dissolved)}$ reduction at the cathode and carbon oxidation at the anode.

4. Conclusions

In this work, a commercially available carbon cloth electrode is repetitively oxidized using a wetting-drying procedure. Examining the effluent pH verifies conversions in surface charged sites of the carbon electrode from positive to negative. Moreover, E_{PZC} is estimated into a potential distribution diagram via the mD model with chemical surface charge. CDI testing configured with symmetric electrode pairs shows that salt removal performance became efficient when the electrode possesses equal positive and negative chemical surface charges or a net chemical surface charge of zero. By mapping the E_{PZC} along with E_{+}, E_{-}, and E_{o}, it is found that ineffectiveness of salt removal is due to the electronic charge consumed to repel co-ionic charge at the intermediate stage, resulting from the driving force of $|E_{PZC} - E_{o}|$. In addition, Faradaic reactions at the electrodes are discussed based upon pH responses during charging and discharging. Finally, it is believed that, through this work, knowledge of the potential distribution along with charge balances can be extended to describe salt separation performance of a CDI cell configured with asymmetric carbon electrode pairs, *e.g.*, enhanced and extended-voltage CDI effects resulting from an anode with positive chemical surface charge paired with a cathode with negative chemical surface charge.[3]

Conflicts of Interest

There are no conflicts of interest to declare.

Acknowledgement

This work is supported by the Crosscutting Research, National Energy Technology Laboratory, U.S. Department of Energy (DE-FE0031555).

References

1. M. A. Shannon, P. W. Bohn, M. Elimelech, J. G. Georgiadis, B. J. Mariñas and A. M. Mayes, Science and technology for water purification in the coming decades, *Nature*, 2008, **452**, 301.
2. M. E. Suss, S. Porada, X. Sun, P. M. Biesheuvel, J. Yoon and V. Presser, Water desalination via capacitive deionization: what is it and what can we expect from it?, *Energy Environ. Sci.*, 2015, **8**, 2296-2319.
3. X. Gao, S. Porada, A. Omosebi, K. L. Liu, P. M. Biesheuvel and J. Landon, Complementary surface charge for enhanced capacitive deionization, *Water Res.*, 2016, **92**, 275-282.
4. P. Srimuk, M. Zeiger, N. Jäckel, A. Tolosa, B. Krüner, S. Fleischmann, I. Grobelsek, M. Aslan, B. Shvartsev and M. E. Suss, Enhanced performance stability of carbon/titania hybrid electrodes during capacitive deionization of oxygen saturated saline water, *Electrochim. Acta*, 2017, **224**, 314-328.
5. T. Wu, G. Wang, F. Zhan, Q. Dong, Q. Ren, J. Wang and J. Qiu, Surface-treated carbon electrodes with modified potential of zero charge for capacitive deionization, *Water Res.*, 2016, **93**, 30-37.
6. P. Srimuk, L. Ries, M. Zeiger, S. Fleischmann, N. Jäckel, A. Tolosa, B. Krüner, M. Aslan and V. Presser, High performance stability of titania decorated carbon for desalination with capacitive deionization in oxygenated water, *RSC Adv.*, 2016, **6**, 106081-106089.
7. J. J. Wouters, J. J. Lado, M. I. Tejedor-Tejedor, R. Perez-Roa and M. A. Anderson, Carbon fiber sheets coated with thin-films of SiO2 and γ-Al2O3 as electrodes in capacitive deionization: Relationship between properties of the oxide films and electrode performance, *Electrochim. Acta*, 2013, **112**, 763-773.
8. J. Yang, L. Zou and N. R. Choudhury, Ion-selective carbon nanotube electrodes in capacitive deionisation, *Electrochim. Acta*, 2013, **91**, 11-19.
9. A. C. Arulrajan, D. L. Ramasamy, M. Sillanpää, A. van der Wal, P. M. Biesheuvel, S. Porada and J. E. Dykstra, Exceptional Water Desalination Performance with Anion-Selective Electrodes, *Adv. Mater.*, 2019, 1806937.
10. A. Omosebi, X. Gao, N. Holubowitch, Z. Li, J. Landon and K. Liu, Anion Exchange Membrane Capacitive Deionization Cells, *J. Electrochem. Soc.*, 2017, **164**, E242-E247.
11. I. Cohen, E. Avraham, Y. Bouhadana, A. Soffer and D. Aurbach, The effect of the flow-regime, reversal of polarization, and oxygen on the long term stability in capacitive de-ionization processes, *Electrochim. Acta*, 2015, **153**, 106-114.
12. G. J. Doornbusch, J. E. Dykstra, P. M. Biesheuvel and M. E. Suss, Fluidized bed electrodes with high carbon loading for water desalination by capacitive deionization, *J. Mater. Chem. A*, 2016, **4**, 3642-3647.
13. S. Kim, J. Lee, C. Kim and J. Yoon, Na2FeP2O7 as a Novel Material for Hybrid Capacitive Deionization, *Electrochim. Acta*, 2016, **203**, 265-271.
14. J. Lee, S. Kim, C. Kim and J. Yoon, Hybrid capacitive deionization to enhance the desalination performance of capacitive techniques, *Energy Envir. Sci.*, 2014, **7**, 3683-3689.
15. X. Gao, A. Omosebi, J. Landon and K. Liu, Voltage-Based Stabilization of Microporous Carbon Electrodes for Inverted Capacitive Deionization, *J. Phys. Chem. C*, 2018, **122**, 1158-1168.
16. X. Gao, A. Omosebi, N. Holubowitch, A. Liu, K. Ruh, J. Landon and K. Liu, Polymer-coated composite anodes for efficient and stable capacitive deionization, *Desalination*, 2016, **399**, 16-20.

17. B. Shapira, E. Avraham and D. Aurbach, Side Reactions in Capacitive Deionization (CDI) Processes: The Role of Oxygen Reduction, *Electrochim. Acta*, 2016, **220**, 285-295.
18. N. Holubowitch, A. Omosebi, J. Landon and K. Liu, Quasi‐steady state polarization reveals the interplay of capacitive and faradaic processes in capacitive deionization, *ChemElectroChem*, 2017, **4**, 2404-2413.
19. C. Zhang, D. He, J. Ma, W. Tang and T. D. Waite, Faradaic reactions in capacitive deionization (CDI) - problems and possibilities: A review, *Water Res.*, 2018, **128**, 314-330.
20. X. Gao, A. Omosebi, J. Landon and K. Liu, Surface charge enhanced carbon electrodes for stable and efficient capacitive deionization using inverted adsorption–desorption behavior, *Energy Environ. Sci.*, 2015, **8**, 897-909.
21. X. Gao, A. Omosebi, J. Landon and K. Liu, Enhanced Salt Removal in an Inverted Capacitive Deionization Cell Using Amine Modified Microporous Carbon Cathodes, *Environ. Sci. Technol.*, 2015, **49**, 10920-10926.
22. X. Gao, A. Omosebi, N. Holubowitch, J. Landon and K. Liu, Capacitive deionization using alternating polarization: effect of surface charge on salt removal, *Electrochim. Acta*, 2017, **233**, 249-255.
23. Y. Qu, P. G. Campbell, L. Gu, J. M. Knipe, E. Dzenitis, J. G. Santiago and M. Stadermann, Energy consumption analysis of constant voltage and constant current operations in capacitive deionization, *Desalination*, 2016, **400**, 18-24.
24. Y. A. C. Jande and W. S. Kim, Desalination using capacitive deionization at constant current, *Desalination*, 2013, **329**, 29-34.
25. S. A. Hawks, J. M. Knipe, P. G. Campbell, C. K. Loeb, M. A. Hubert, J. G. Santiago and M. Stadermann, Quantifying the flow efficiency in constant-current capacitive deionization, *Water Res.*, 2018, **129**, 327-336.
26. P. M. Biesheuvel, H. Hamelers and M. Suss, Theory of Water Desalination by Porous Electrodes with Immobile Chemical Charge, *Colloids Interf. Sci. Commun.*, 2015, **9**, 1-5.
27. P. M. Biesheuvel, S. Porada, M. Levi and M. Z. Bazant, Attractive forces in microporous carbon electrodes for capacitive deionization, *J. Solid State Electrochem.*, 2014, **18**, 1365-1376.
28. P. Biesheuvel, Theory of expansion of porous carbon electrodes in aqueous solutions according to the Donnan model, *arXiv preprint arXiv:1702.05310*, 2017.
29. R. Zhao, P. M. Biesheuvel, H. Miedema, H. Bruning and A. van der Wal, Charge Efficiency: A Functional Tool to Probe the Double-Layer Structure Inside of Porous Electrodes and Application in the Modeling of Capacitive Deionization, *J. Phys. Chem. Lett.*, 2010, **1**, 205-210.
30. M. E. Suss, Size-Based Ion Selectivity of Micropore Electric Double Layers in Capacitive Deionization Electrodes, *Journal of The Electrochemical Society*, 2017, **164**, E270-E275.
31. E. Avraham, Y. Bouhadana, A. Soffer and D. Aurbach, Limitation of Charge Efficiency in Capacitive Deionization: I. On the Behavior of Single Activated Carbon, *J. Electrochem. Soc.*, 2009, **156**, P95-P99.
32. E. Avraham, M. Noked, Y. Bouhadana, A. Soffer and D. Aurbach, Limitations of Charge Efficiency in Capacitive Deionization: II. On the Behavior of CDI Cells Comprising Two Activated Carbon Electrodes, *J. Electrochem. Soc.*, 2009, **156**, P157-P162.
33. E. Avraham, M. Noked, Y. Bouhadana, A. Soffer and D. Aurbach, Limitations of charge efficiency in capacitive deionization processes III: The behavior of surface oxidized activated carbon electrodes, *Electrochim. Acta*, 2010, **56**, 441-447.

34. A. J. Bard and L. R. Faulkner, *Electrochemical Methods - Fundamentals and Applications*, John Wiley & Sons, New York, 2nd edn., 2001.
35. M. D. Levi, S. Sigalov, D. Aurbach and L. Daikhin, In Situ Electrochemical Quartz Crystal Admittance Methodology for Tracking Compositional and Mechanical Changes in Porous Carbon Electrodes, *J. Phys. Chem. C*, 2013, **117**, 14876-14889.
36. C.-T. Hsieh and H. Teng, Influence of oxygen treatment on electric double-layer capacitance of activated carbon fabrics, *Carbon*, 2002, **40**, 667-674.
37. C. Lastoskie, K. E. Gubbins and N. Quirke, Pore size distribution analysis of microporous carbons: a density functional theory approach, *J. Phys. Chem.*, 1993, **97**, 4786-4796.
38. A. Hemmatifar, D. I. Oyarzun, J. W. Palko, S. A. Hawks, M. Stadermann and J. G. Santiago, Equilibria model for pH variations and ion adsorption in capacitive deionization electrodes, *Water Res.*, 2017, **122**, 387-397.
39. K. Kinoshita, *Carbon - Electrochemical and Physicochemical Properties*, John Wiley & Sons, New York, 1988.
40. T. Szabó, E. Tombácz, E. Illés and I. Dékány, Enhanced acidity and pH-dependent surface charge characterization of successively oxidized graphite oxides, *Carbon*, 2006, **44**, 537-545.
41. B. Stuart, Infrared Spectroscopy: Fundamentals and Applications. 2004, *JohnWiley & Sons, Ltd*.
42. J. L. Figueiredo, M. F. R. Pereira, M. M. A. Freitas and J. J. M. Órfão, Modification of the surface chemistry of activated carbons, *Carbon*, 1999, **37**, 1379-1389.
43. T. Kim and J. Yoon, CDI ragone plot as a functional tool to evaluate desalination performance in capacitive deionization, *RSC Adv.*, 2015, **5**, 1456-1461.
44. Y. Oren, Capacitive deionization (CDI) for desalination and water treatment — past, present and future (a review), *Desalination*, 2008, **228**, 10-29.
45. D. He, C. E. Wong, W. Tang, P. Kovalsky and T. D. Waite, Faradaic Reactions in Water Desalination by Batch-Mode Capacitive Deionization, *Environ. Sci. Technol. Lett.*, 2016, **3**, 222-226.
46. S. Maass, F. Finsterwalder, G. Frank, R. Hartmann and C. Merten, Carbon support oxidation in PEM fuel cell cathodes, *J. Power Sources*, 2008, **176**, 444-451.

Table of Contents Entry

Scenarios (a)-(c) are created to study the effect of chemical surface charge of carbon electrodes on capacitive deionization using symmetric carbon electrode pairs.